Biosensors and Bioelectronics 188 (2021) 113340

Contents lists available at ScienceDirect

Biosensors and Bioelectronics

journal homepage: www.elsevier.com/locate/bios

Regenerative field effect transistor biosensor for in vivo monitoring of dopamine in fish brains

Na Liu [a,c,1], Xueping Xiang [b,1], Lei Fu [d,1], Qiang Cao [a,c], Rong Huang [a], Huan Liu [a], Gang Han [a], Lidong Wu [a,*]

[a] Key Laboratory of Control of Quality and Safety for Aquatic Products, Chinese Academy of Fishery Sciences, Beijing, 100141, China
[b] Department of Pathology, The Second Affiliated Hospital, School of Medicine, Zhejiang University, Hangzhou, 310009, China
[c] College of Food Science and Technology, Shanghai Ocean University, Shanghai, 201306, China
[d] Bionic Sensing and Intelligence Center, Institute of Biomedical and Health Engineering, Shenzhen Institutes of Advanced Technology, Chinese Academy of Sciences, Shenzhen, 518055, China

ARTICLE INFO

Keywords:
Fe_3O_4@AuNPs
FET biosensor
Magnetic field
Dopamine
Fish brain

ABSTRACT

The detection of dopamine, one of the neurotransmitters in cerebral physiology, is critical in studying brain activities and understanding brain functions. However, regenerative biosensor for monitoring dopamine in the progress of physiological and pathological events is still challenging, due to lack of the platform for repetitive on-line detection-regeneration cycle. Herein, we have developed a regenerated field effect transistor (FET) combined with in vivo monitoring system. In this biosensor, gold-coated magnetic nanoparticles (Fe_3O_4@AuNPs) acts as a regenerated recognition unit for dopamine. Just by simple removal of a permanent magnet, dopamine on the biosensor interface are catalyzed by tyrosinase, thus achieving the regeneration of the biosensor. As a result, this FET biosensor not only reveals high sensitivity and selectivity, but also exhibits excellent stability after 15 regeneration processing. This biosensor is capable of monitor dopamine with a linear range between 1 μmol L^{-1} and 120 μmol L^{-1} and low detection limit (DL) of 3.3 nmol L^{-1}. Then, the platform has been successfully applied in dopamine analysis in fish brain under global cerebral cortical neurons. This FET biosensor is the first to on-line and remote control the sensitivity and DL by permanent magnet. It opens the door to reusable, inexpensive and large-scale productions.

1. Introduction

During the past decades, technological advances have bloomed to fields such as artificial intelligence, internet of things and brain-computer interface, thus stimulating a strongly growing demand for regenerative sensor devices to specifically detect, quantify, and monitor varieties of biological and chemical species. Field-effect transistors (FETs) as one of the most promising platforms provide a tailored solution to this demand (Artyukhin et al., 2006; Chen et al., 2009; Elnathan et al., 2012). FETs modified with target-specific receptors could rapidly detect target molecules (Chen et al., 2019a; Cheung et al., 2019; Magliulo et al., 2015). Signal transduction and amplification in FET-based biosensor depend on electrostatic gating of semiconductor channels by target-receptor interactions (Belyanina et al., 2017; Chen et al., 2019b; Nakatsuka et al., 2018; Singh et al., 2019). Thus, the receptor-modified FETs should overcome two fundamental limits: one of the limits is that small target molecules with few or no charges have minimal impact on transistor transconductance unless they trigger conformational changes in charged receptors or induce enzymatic reaction to extremely amplify the response signal (Hartl et al., 2008; Li et al., 2011; Wu et al., 2014). Another limit in receptor-modified FETs is the method of regenerating the device to lower the device price (Gao et al., 2012; Khoshfetrat and Mehrgardi, 2017; Kwon et al., 2012; Vijayalakshmi et al., 2008).

Dopamine as one of the important neurotransmitters is produced by the dopaminergic neurons in the brain (Vasudevan et al., 2019). Owing to this importance of dopamine, insufficient dopamine levels in the brain could lead to severe neurological diseases such as Parkinson's disease, and schizophrenia, etc (Rakovska et al., 2019). To achieve specific sensing of no charge molecules (dopamine), FETs biosensors can involve

* Corresponding author.
E-mail address: wulidong19849510@hotmail.com (L. Wu).
[1] Authors equally contribution to this work.

https://doi.org/10.1016/j.bios.2021.113340
Received 23 November 2020; Received in revised form 27 March 2021; Accepted 11 May 2021
Available online 17 May 2021

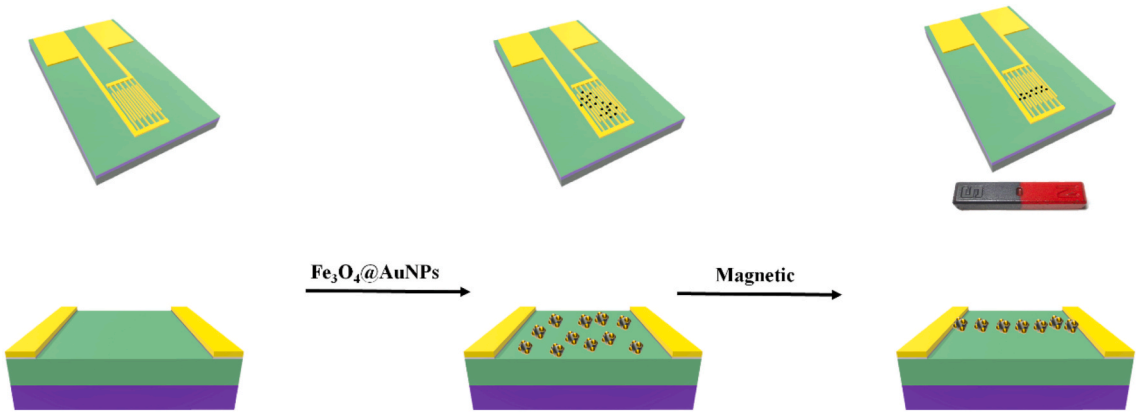

Scheme 1. Schematic of magnet controlled Fe_3O_4@AuNPs nanoparticles formation magnetic bridge through source to the drain of the FET.

structural and functional integration of bio-receptors, such as enzymes (Chae et al., 2018; Choi and Yau, 2009; Ogata et al., 2004), antibodies, aptamers, etc (Hammock et al., 2014; Melzer et al., 2016; Ordinario et al., 2014). The integration of enzymes and FETs is an attractive and potential approach for the detection of specific substrates. Enzyme functionalized FETs (EN-FETs) biosensors can selectively react with target molecules as substrates (Mao et al., 2017), where the enzymatic catalysis leads to perturbation of electric potential at the FETs channel/electrolyte interface, or changes of the charge carrier density and the conductance of FETs devices as readouts instantly (Hafez et al., 2019;

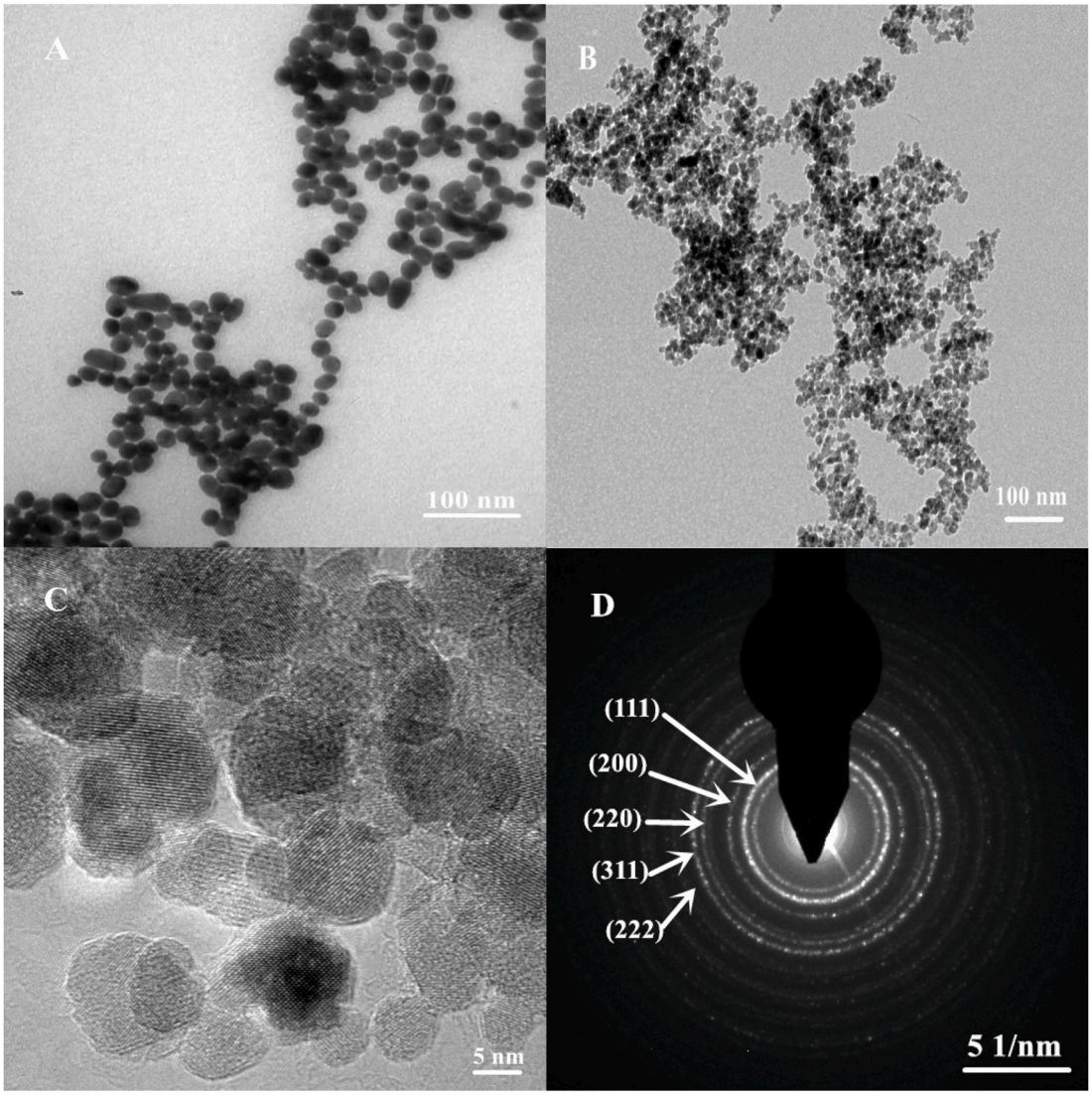

Fig. 1. TEM image of (A) Fe_3O_4 nanoparticles, (B) Fe_3O_4@AuNPs nanoparticles, (C) enlarged image of Fe_3O_4@AuNPs nanoparticles and (D) Electron diffraction pattern of the selected area from the Fe_3O_4@AuNPs nanoparticles.

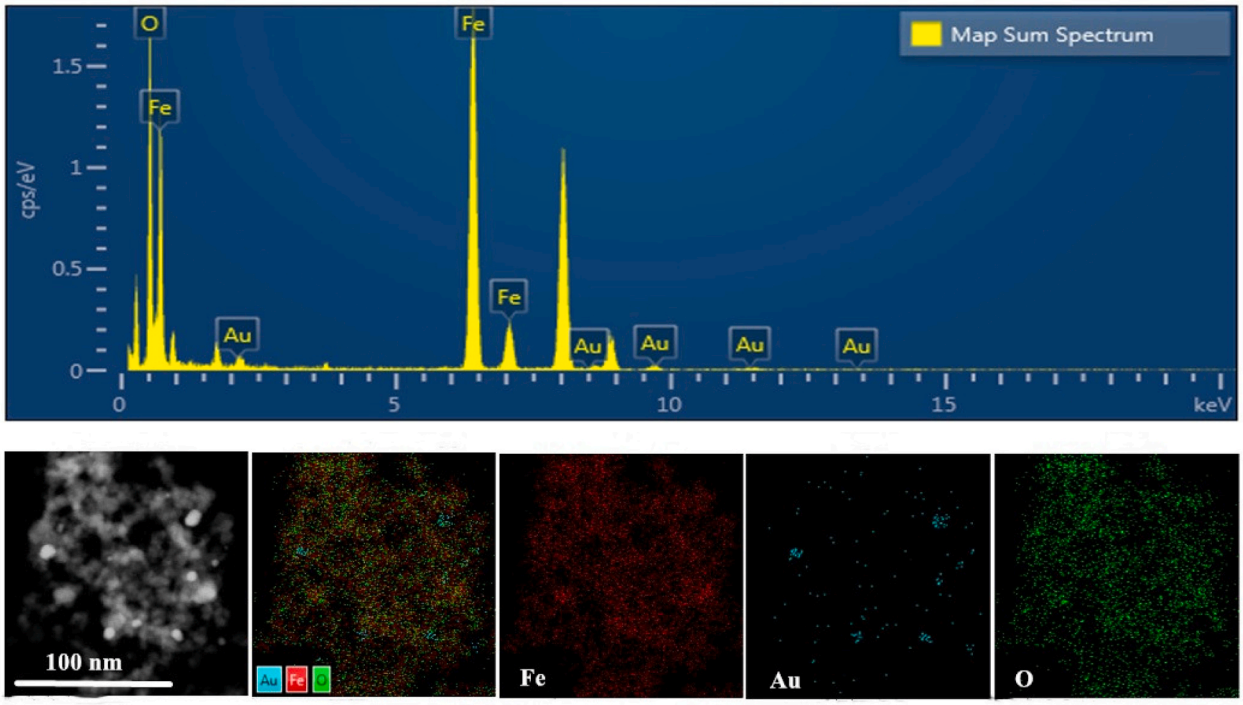

Fig. 2. Elemental mapping of Fe_3O_4@AuNPs.

Hammock et al., 2014; Yoon et al., 2008). To overcome another challenge in regenerating the EN-FETs, a regenerative recognition unit is immobilized on the FETs channel (Caras et al., 1985; Kamahori et al., 2007; Kergoat et al., 2012). Currently, low-dimensional materials (such as carbon nanotubes, graphene and molybdenum disulfide) are usually treated as the preferred channel materials for FETs biosensors (Surya et al., 2020; Yang et al., 2005). However, the stringent conditions of low-dimensional materials transfer and fabrication technologies limit their applications in real-time monitoring and regeneration (Gao et al., 2010; Park et al., 2012).

In this work, we designed a regenerated FETs biosensor to overcome these challenges. Gold coated magnetic nanoparticles (Fe_3O_4@AuNPs) selected as FETs amplifier and regenerative unit and can remotely controlled by a permanent magnet. A nanometer-thin HfO_2 FETs was prepared by atomic layer deposition (ALD). As shown in Scheme 1, the magnetic field remotely controlled the paramagnetic Fe_3O_4@AuNPs forming regenerative unit. Through adjusting distance between the magnet and the HfO_2 FETs devices, the sensitivities and detection limits of the EN-FETs biosensors for dopamine were easily controlled. Hence, combination the advantage of magnetic Fe_3O_4@AuNPs and FETs provides a promising and controllable method to construct a regenerative EN-FETs biosensor.

2. Experimental section

Chemicals: $FeCl_2$, $FeCl_3$, ammonium hydroxide, chloroauric acid and ethanol were purchased from Macklin (Shanghai, China). Tyrosinase were purchased from Sigma-Aldrich (Beijing, China). All chemicals were used as received without further purification.

Instrumentation: Transmission electron microscopy (TEM) images were obtained from a HT7700 TEM (Hitachi Co. Ltd., Japan) with an accelerating voltage of 120 kV. Scanning electron microscopy (SEM) images were obtained by a SU8220 SEM (Hitachi Co. Ltd., Japan) with an accelerating voltage of 1 kV. Fourier transform infrared spectroscopy (FTIR) was obtained by an IR Tracer-100 (Shimadzu, Co. Ltd. Japan). UV/Vis spectra were recorded by an Analytik Jena Specord 210 plus spectrophotometer (Jena Co. Ltd., Germany). The zeta potential was measured by a Zetasizer Nano ZS (Malvern Panalytical, UK). 18.2 MΩ deionized water was obtained from Milli-Q® Type 1 Ultrapure Water Systems (Millipore, USA). The drain-source currents were obtained from Agilent B1500a assisted with Cascade Summit 12000 probe station.

Synthesis of Fe_3O_4@AuNPs. Fe_3O_4@AuNPs were synthesized by coprecipitation of Fe (II) and Fe (III) salt in alkaline medium and then reduction of Au^{3+} onto the Fe oxide surfaces: First, 50 mL of deionized water and ethanol (volume 1:1) containing Fe(II) and Fe(III) chlorides (Fe^{II}/Fe^{III} ratio = 1:4) with 1.0 mL $NH_3{\cdot}H_2O$ as the reductant was placed in a 250 mL round-bottom flask (with nitrogen gas) and stirred at 25 °C for 2 h. The product was washed by deionized water for 5 times and centrifuged under 10000 rpm to obtain the Fe_3O_4 nanoparticles. Subsequently, the Fe_3O_4 nanoparticles were mixed with chloroauric acid and reducing agent (sodium citrate) heated at 90 °C and stirred for 1 h. In this procedure, the Au layer was formed by reduction of Au^{3+} onto the Fe_3O_4 nanoparticles surface. Finally, the Fe_3O_4@AuNPs product was collected by applying magnetic field, washed with ethanol for three times and dispersed in 50 mL ethanol for further use.

Preparation of the FET chip. The fabrication process of a FET chip was shown in Scheme S1 and tested in a super clean room to ensure the yield rates. First, a 300 nm SiO_2 layer was evaporated on the silicon wafer by thermal oxygen method. Following, the SiO_2 layer was cleaned by nitrogen gas. Second, the photoresist was rotated on the SiO_2 layer, and the electrode model was transferred to the photoresist by lithography method. Oxygen plasma etching was used to move the residual of photoresist. Third, a 5 nm HfO_2 layer was deposited on the SiO_2 layer by ALD method, a 10 nm Ti layer was deposited on SiO_2 layer by electron beam evaporation, and gold electrode was deposited on the Ti layer. Finally, the FET chip was obtained after lift-off step.

Fabrication of Fe_3O_4@AuNPs based FET chip. FETs become attractive biosensors when the standard metal oxide FETs redesigned by replacing the gate electrode with a reference electrode dipped in solution to make a contact with the gate oxide. Fe_3O_4@AuNPs solution was coated on the FETs chip as follows: 10 μL of 0.5 mg mL^{-1} Fe_3O_4@AuNPs solution was dropped on the channel of the FETs chip. The density of the Fe_3O_4@AuNPs was remotely controlled by the magnetic field. Subsequently, 0.05 mg mL^{-1} tyrosinase was immobilized on the previous

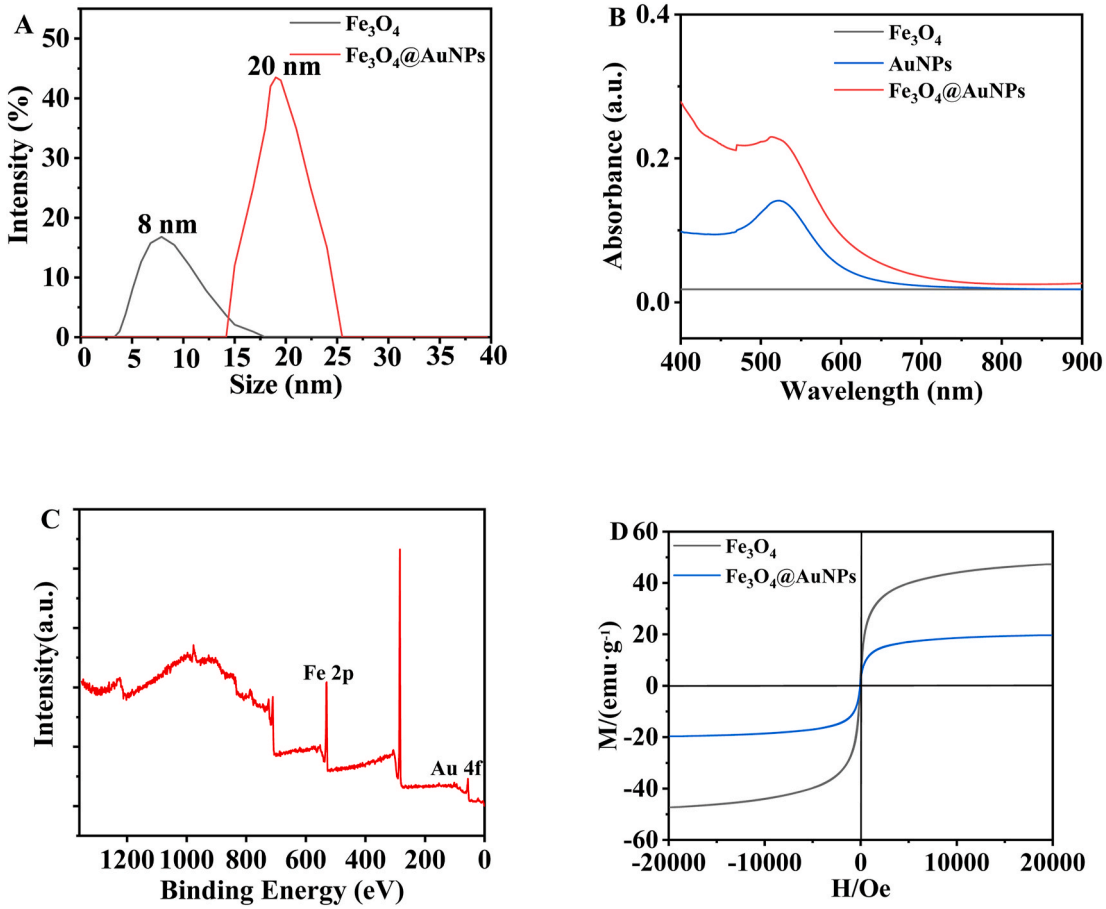

Fig. 3. (A) DLS number of Fe_3O_4 nanoparticles and Fe_3O_4@AuNPs nanoparticles, (B) UV–vis spectrum of Fe_3O_4, AuNPs and Fe_3O_4@AuNPs, (C) XPS spectrum of Fe_3O_4@AuNPs, and (D) The magnetization curves of Fe_3O_4, and Fe_3O_4@AuNPs.

obtained FETs chip, and the chip was dried by nitrogen stream. The source-drain current (I_{ds}) was monitored with different gate voltage (V_g) to investigate the gate control effect of the device.

Safety Considerations. MSDS information for chemicals must be consulted, and precautions need to be taken while handling them (i.e., wearing gloves, eye protection and a mask).

3. Results and discussion

Morphology characterization of the Fe_3O_4@AuNPs. The morphologies and sizes of the Fe_3O_4@AuNPs nanoparticles were analyzed by TEM, DLS and UV–vis. Fig. 1A and B showed that the synthesized Fe_3O_4 and Fe_3O_4@AuNPs nanoparticles appeared nearly a spherical shape. Fig. 1C and D showed the high resolution TEM image and diffraction pattern of the Fe_3O_4@AuNPs. The high resolution TEM image displayed one of nanoplate structure with well-resolved (111) type crystallographic planes (measured D-spacing of approximate 0.3 nm). The diffraction pattern of Fe_3O_4@AuNPs displayed rings corresponding to the (111), (200), (220), (311) and (222) reflections of the face-centered-cubic structure of gold. The EDX analysis was shown in Fig. 2. It could be observed that there was Au element dispersed around the Fe and O elements. This indicated that the Au nanoparticles had covered on the surface of Fe_3O_4.

As shown in Fig. 3A, their sizes increased from 8 nm to 20 nm. The increase of nanoparticles diameter was due to coating of gold nanoparticles. As shown in Fig. S1, the obtained Fe_3O_4@AuNPs nanoparticles were easily enriched nearby the magnet in water solution, proving that these nanoparticles would be successfully employed as material for rapid constructing a FET biosensor. Fig. 3B showed the UV–vis spectra of the Fe_3O_4, AuNPs and Fe_3O_4@AuNPs. There was a significant absorbance peak at 530 nm ascribed to the AuNPs but no significant absorbance peak in the Fe_3O_4 nanoparticles ranging from 400 to 900 nm. After coating with the AuNPs, a surface plasmon band was observed in the Fe_3O_4@AuNPs approximately 537 nm. The similar absorbance peak confirmed a successfully modified with AuNPs. As a magnet was placed near the wall of the spectrometric cell, no absorbance peak could be observed. This phenomenon confirmed that the absorbance peak at 530–540 nm was due to the Fe_3O_4@AuNPs not the pure AuNPs. We also employed XPS for further analysis of surface chemistry of Fe_3O_4@AuNPs. The binding energy of electrons of an atom was sensitive to the local electronic state of adjacent atoms and provided information about binding and coordination of functional groups. As shown in Fig. 3C, the binding energy of the Fe^{2+} and Fe^{3+} was found at approximately 710.8 and 724.5 eV, respectively. The binding energy of the Au 4f was found at 92.5 eV. The XPS results provided evidence for the formation of Fe_3O_4 and AuNPs. The magnetic performance was investigated using a superconducting quantum interference device at 300 K in Fig. 3D. The magnetic saturation of Fe_3O_4 was approximate 50 emu g^{-1}. While the magnetic saturation of Fe_3O_4@AuNPs was decreased to 20 emu g^{-1}. Both of nanomaterials enabled instantaneous magnetic separation.

Magnetic remote manipulation for the fabrication of EN-FET biosensors. In conjunction with conventional fabrication methods, wafer-scale fabrication of FET biosensor was made by several large-scale nanowire-positioning techniques such as contact printing and physical manipulation (Fan et al., 2008). We demonstrated the use of a magnetic remote manipulation post-processing method to form EN-FET biosensors with well-controlled morphologies. Fig. S2 showed the

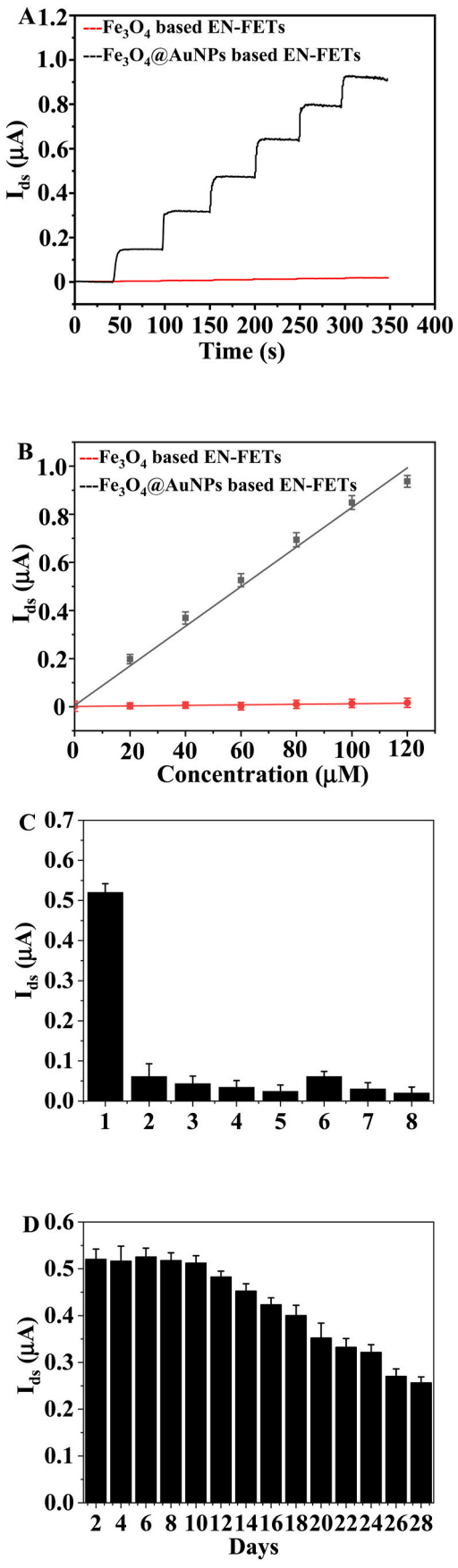

(caption on next column)

Fig. 4. (A) I_{ds} of the Fe_3O_4@AuNPs based EN-FET biosensor and the Fe_3O_4 based EN-FET biosensor under magnet for 20 μmol L^{-1} of dopamine detection. (B) The linear curves of I_{ds} and dopamine concentration. (C) The Fe_3O_4@AuNPs based EN-FET biosensor screen dopamine, DOPA, 4-propylcatechol, norepinephrine, 3,4-dihydroxybenzoic acid, 2,4-dihydroxyphenol, epinephrine and gallic acid at 60 μmol L^{-1}. (D) The relationship between storage time and I_{ds} of the Fe_3O_4@AuNPs based EN-FET biosensor at 4 °C.

photograph of FET chip compared with 50 cents coin. The EN-FETs were fabricated by using interdigitated gold microelectrodes with 2.5 μm channels. As shown in Scheme 1, in this configuration the narrow channel was bridging the source-drain electrode pair by Fe_3O_4@AuNPs. Bridging nanochannels were physically constructed by employing magnet under the electrode center. Using this method, the fabrication process was simple and efficient. Under the magnetic attraction, a nanobridge rapidly connected source and drain contact of the FETs. Thus, Fe_3O_4@AuNPs nanoparticles were well-organized on the FETs channel/electrolyte interface via magnetic attraction for adjusting signal output.

Cyclic Voltammetry (CV) is a sensitive technique to monitor the formation of the adsorption layer on the FET biosensor. Fig. S3 showed the CVs of the bare FET biosensor, Fe_3O_4@AuNPs and Fe_3O_4@AuNPs based EN-FET biosensor in the 100 mM PBS solution. It showed that there were no peaks on the bare FET biosensor. In contract, a redox peak was observed on EN-FET biosensor. After introduction of Fe_3O_4@AuNPs materials, a significantly well-defined redox peak was observed on Fe_3O_4@AuNPs based EN-FET biosensor. This difference resulted from the fact that Fe_3O_4@AuNPs could significantly enhance the direct electron transfer between the tyrosinase and the FET biosensor. It indicated that tyrosinase was successfully immobilized on the FET biosensor.

Electrical characterization was subsequently performed by Agilent B1500a to obtain device I–V characteristics. To utilize Fe_3O_4@AuNPs as a signal transducer in the electronic EN-FET biosensor system, we introduced a tyrosinase which can selectively catalyze dopamine with high affinity. The reaction mechanism between tyrosinase and dopamine: dopamine was hydroxylated to dopa-quinone in the presence of tyrosinase. The dopa-quinone could be electrochemical reduced to dopamine for the next electrode reaction. As shown in Scheme S2, the abundant H+ produced by tyrosinase catalysis reaction could increase the current of the FET sensor. To evaluate magnetic field remotely controlled effects, the current-voltage (I–V) curves were tested. Fig. S4A showed the I–V curves of the Fe_3O_4@AuNPs based TYR-FETs with or without employing magnet. Without magnet, this FET biosensor showed no minimum conductivity point. Under magnet field, there was an obvious minimum conductivity point at approximate 0.2 V. The difference of the curves was presumably due to the difference in the resistance. The results indicated that employing magnet connected the source-drain electrode pair and the immobilization of the Fe_3O_4@AuNPs nanoparticles under magnet resulting in a reliable electrical contact. As shown in Fig. S4B, I_{ds} was positively enhanced with positively increasing V_g, meaning that the stable n-type (electron-transporting) behavior took place after employing magnet (Garrido et al., 2008). In addition, as shown in the SEM and optical images of Fig. S5, the dispersed Fe_3O_4@AuNPs nanoparticles bridged linearly between the source and drain electrodes, which was attributed to remotely control by the magnet field. Remotely controlled the properties of Fe_3O_4@AuNPs based EN-FETs by magnetic field.

Dopamine molecules are catalyzed by tyrosinase, which in turn transduces a signal in the EN-FET biosensor. Such enzyme reaction can affect the charge-carrier density on the surface of Fe_3O_4@AuNPs, and thus it may allow label-free recognition of target molecules (dopamine) on the FET configuration. A typical response of a Fe_3O_4@AuNPs@CYS based EN-FETs and EN-FETs under magnet attraction was shown in Fig. 4A. As different concentrations of dopamine were added on the surface of EN-FET, the I_{ds} value of the EN-FET were measured. The

Table 1
Analysis of dopamine by different reported methods.

Sensors	Detection limit (nmol L^{-1})	Dynamic range (μmol L^{-1})	Reference
Fe_3O_4@AuNPs based EN-FET	3.3	1–120	Present work
Graphene based sensor	110	0.3–56.8	He et al. (2020)
CNTs and AuCo nanoparticles based sensor	150	1.25–281	Bai et al. (2020)
MoS_2 with manganese based sensor	5	0.05–5	Lei et al. (2020)
Molecularly imprinted polymer with gold based sensor	300	2–160	Li et al. (2020)
FeMn nanoparticles based sensor	5.3	0.020–700	Annalakshmi et al. (2020)

results showed that the I_{ds} values increased with addition of dopamine, and the response signal of Fe_3O_4@AuNPs based EN-FETs was significantly higher than that of EN-FETs.

As an EN-FETs biosensor, sensitivity, selectivity and detection limit are important parameters to evaluate the biosensor performances. Sensitivity is the magnitude of sensor transduction signal change versus the change of analyte concentration (Singh et al., 2019). The sensitivities of EN-FETs biosensors were evaluated using the linear slope at a certain concentration (as shown in Fig. 4B). The sensitivity of Fe_3O_4@AuNPs based EN-FETs biosensor was 3.16 mA/M, which was approximately 70 times higher than that of the Fe_3O_4 based EN-FETs biosensor ($4.68*10^{-2}$ mA/M). The calibration curve of the Fe_3O_4@AuNPs based EN-FETs biosensor showed a linear response from 1 μmol L^{-1} to 120 μmol L^{-1}. It indicated that the magnetic Fe_3O_4@AuNPs played a key role in improving the sensitivity of the EN-FETs biosensor. Selectivity is the ability of a biosensor to detect a specific analyte in a sample containing other admixtures and contaminants. To explore the selectivity, 60 μmol L^{-1} dopamine and dopamine analogues (DOPA, norepinephrine, 4-propylcatechol, 3,4-dihydroxybenzoic acid, gallic acid, 2,4-dihydroxyphenol, and epinephrine) were used to evaluate the specificity of the Fe_3O_4@AuNPs based EN-FETs biosensor in Fig. 4C. Their chemical structures were shown in Fig. S6. Negligible responses were observed by the Fe_3O_4@AuNPs based EN-FETs biosensor when dopamine analogues were added at the same concentration of dopamine. The results clearly indicated that this EN-FET biosensor possessed an excellent selectivity for dopamine against other dopamine analogues. The detection limit of this biosensor was another important parameter, and the detection limit (S/N = 3) of the Fe_3O_4@AuNPs based EN-FETs and the Fe_3O_4 based EN-FETs biosensors were calculated as 3.3 nmol L^{-1} and 10 μmol L^{-1}, respectively. As shown in Tables 1 and S1, its detection limit was lower than previous report. Furthermore, the Fe_3O_4@AuNPs based EN-FETs biosensor was stored in a refrigerator at 4 °C. The stability of this FET biosensor was monitored through the addition of 60 μmol L^{-1} dopamine and recorded their response changes in Fig. 4D. The initial signal of the Fe_3O_4@AuNPs based EN-FETs biosensor decreased to approximate 50% after four weeks. The initial signal decrease of Fe3O4@AuNPs ENFETs was ascribed to the loss of tyrosinase activity on the FET sensor. After tyrosinase immobilized on the Fe_3O_4@AuNPs materials, there were only electrostatic attraction between tyrosinase and Fe_3O_4@AuNPs. Thus, tyrosinase structure was easily broken after four weeks storage.

The Fe_3O_4@AuNPs based EN-FETs biosensor was fabricated by using deposition techniques and remote manipulation by magnetic field. Unlike single-use biosensor, the sensitivity and detection limit of the Fe_3O_4@AuNPs based EN-FETs can be in-site optimization only in single biosensor through remote manipulation by magnetic field strength. It should be stressed that the sensitivity and detection limit of EN-FETs

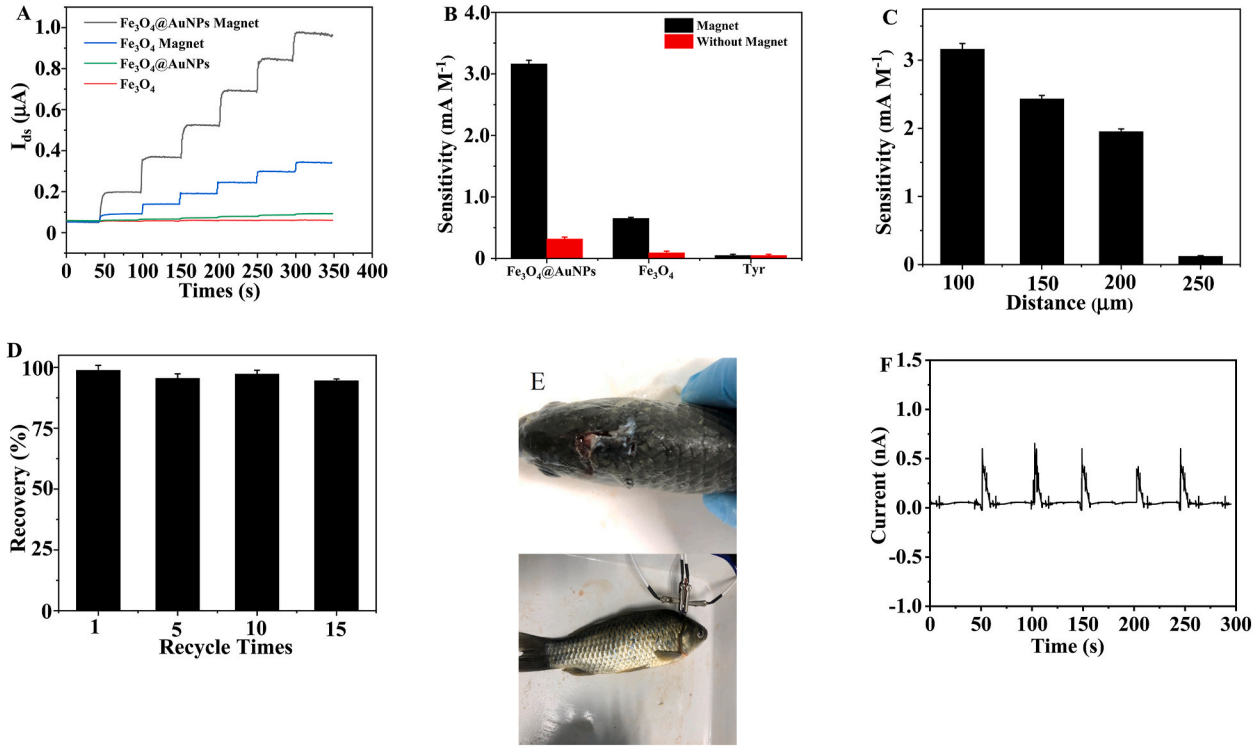

Fig. 5. (A) I_{ds} of the Fe_3O_4@AuNPs based EN-FET biosensor and Fe_3O_4@AuNPs based EN-FET biosensor with or without magnet for 20 μmol L^{-1} of dopamine detection. (B) The sensitivity of the Fe_3O_4@AuNPs, Fe_3O_4 and Tyr based EN-FET biosensors with or without magnet for dopamine. (C) The sensitivity of the Fe_3O_4@AuNPs based EN-FET biosensor for dopamine with different distances of magnet (100, 150, 200 and 250 μm). (D) The recovery number of the EN-FETs biosensor is controlled by magnet after recycled 5, 10, 15 times. (E) Photo of the crucian fish brain and the EN-FET chip setup on the fish brain. (F) The I_{ds} output signal of crucian fish brain monitored by the EN-FET chip.

were influenced by the magnetic field strength. A detailed analysis of these influencing factors was shown in Fig. 5. The I_{ds} curves with magnetic field strength versus dopamine concentration of the Fe_3O_4@AuNPs based EN-FETs biosensors were shown in Fig. 5A and B. It indicated that the magnetic field played as an amplifier and remotely tuned the sensitivity of these biosensors. Without magnetic nanoparticles, the sensitivity of the EN-FET biosensor showed no difference, and it is the lowest sensitivity among these sensors. Furthermore, after modification with Fe_3O_4 or Fe_3O_4@AuNPs, the sensitivity of Fe_3O_4@AuNPs based EN-FETs biosensor (3.16 mA/M) is 3 times higher than that of Fe_3O_4 based EN-FETs biosensor (1.0 mA/M). The magnetic amplifier ratio of Fe_3O_4@AuNPs and Fe_3O_4 based EN-FETs biosensors were 10 and 6, respectively. This conclusion was consistent with previous report (Li et al., 2018; Ye et al., 2018; Zhang et al., 2007).

To achieve on-line optimization the sensitivity of EN-FETs biosensor, remote control of magnet has been taken in account. As shown in Fig. 5C, the sensitivity of the Fe_3O_4@AuNPs based EN-FETs biosensor increased with decreasing the magnet distance. Through controlling the magnet distance, the properties of biosensor could be easily and controllably improved. Without employing magnet, the magnetic nanoparticles on the FETs were randomly distributed, and the sensitivity of EN-FETs was relatively low. When the distance between magnet and the EN-FET was larger than 250 μm, the magnet could not play a role in tuning the sensitivity of the EN-FET. As the distance between magnet and EN-FET gradually shortened, the sensitivity of EN-FET could increase linearly. This was due to the source and drain electrodes bridged by magnetic nanoparticles, and the dipoles aligned vertically along the thickness direction by magnet. The equation for magnetic force was similar to Coulomb's Law. The magnetic force (F) was inversely proportional to the distance squared (i.e., it obeys an inverse square law with distance, $F \propto 1/r^2$). Where r is the distance between the magnet and the EN-FET. In the nanocomposite, the Fe_3O_4 core plays a key role in online optimization the density and morphology of Fe_3O_4@AuNPs on EN-FETs. The AuNPs shell plays as binding sites for the tyrosinase enzyme and can improve the conductivity of Fe_3O_4@AuNPs nanocomposite and sensitivity of EN-FETs sensor.

Furthermore, as shown in Fig. 5D, the Fe_3O_4@AuNPs based EN-FETs biosensor could be easily regenerated. After this EN-FETs chip dipped in the deionic water and ultrasonically washed for 5 min, the EN-FETs chip could be refreshed. After regenerated 15 times, the sensitivities of regenerated Fe_3O_4@AuNPs based EN-FETs only decreased approximate 5%. In this way, the sensitivity of the EN-FET biosensor could be remotely controlled as you wish. This method was crucial for regenerating sensors and other realistic applications. The practicability of the Fe_3O_4@AuNPs based EN-FETs biosensor in the crucian fish brain had been studied (Fig. 5E and F). The fabricated chip was used for dopamine monitoring in crucian fish brain using the source-drain current as output signal. This chip was successfully applied to monitor the concentration of dopamine in fish brain. As shown in Fig. 5F, the output signals of the EN-FET chip were correlated with dopamine concentration in the fish brain.

4. Conclusion

To summarize, we have developed a remotely controlled method for fabrication of EN-FETs biosensor. The magnetic nanoparticles are selected as a controllably conductive bridging material and the sensitivity of EN-FET biosensors can be easily adjusted by magnetic field. With the successful coupling of the magnetism, enzyme, and transistor, the EN-FET biosensors could effectively control. Notably, this EN-FETs biosensor can be easily regenerated only in one EN-FETs chip as you wish. The integrated devices offer a new technical route coupling magnetism and transistor, and greatly enrich the exploration and application in the FET sensor research area, which may be widely employed in sensor, brain-computer interface, and logic device. More novel devices and applications based on our study may be explored in the future.

Credit author statement

The manuscript was written through contributions from all authors. All authors have approved the final version of the manuscript. The authors Liu, Xiang and Fu contributed equally.

Lidong Wu: Funding acquisition; Supervision; Writing - original draft; Writing - review & editing; Project administration

Na Liu, Xueping Xiang and Lei Fu: experiment tests and biochip modification

Rong Huang and Qiang Cao: Data curation

Huan Liu and Gang Han: Writing - review & editing

Declaration of competing interest

The authors declare that they have no known competing financial interests or personal relationships that could have appeared to influence the work reported in this paper.

Acknowledgments

This work was supported by the Central Public-interest Scientific Institution Basal Research Fund, CAFS (No. 2020GH09 and 2020TD75).

Appendix A. Supplementary data

Supplementary data to this article can be found online at https://doi.org/10.1016/j.bios.2021.113340.

References

Annalakshmi, M., Kumaravel, S., Chen, S.M., Chen, T.W., 2020. FeMn layered double hydroxides: an efficient bifunctional electrocatalyst for real-time tracking of cysteine in whole blood and dopamine in biological samples. J. Mater. Chem. B 8 (36), 8249–8260.

Artyukhin, A.B., Stadermann, M., Friddle, R.W., Stroeve, P., Bakajin, O., Noy, A., 2006. Controlled electrostatic gating of carbon nanotube FET devices. Nano Lett. 6 (9), 2080–2085.

Bai, Z., Gao, N., Xu, H., Wang, X., Tan, L., Pang, H., Ma, H., 2020. Construction of an ultra-sensitive electrochemical sensor based on polyoxometalates decorated with CNTs and AuCo nanoparticles for the voltammetric simultaneous determination of dopamine and uric acid. Mikrochim. Acta 187 (8), 483–489.

Belyanina, I.V., Zamay, T.N., Zamay, G.S., Zamay, S.S., Kolovskaya, O.S., Ivanchenko, T. I., Denisenko, V.V., Kirichenko, A.K., Glazyrin, Y.E., Garanzha, I.V., Grigorieva, V.V., Shabanov, A.V., Veprintsev, D.V., Sokolov, A.E., Sadovskii, V.M., Gargaun, A., Berezovski, M.V., Kichkailo, A.S., 2017. In vivo cancer cells elimination guided by aptamer-functionalized gold-coated magnetic nanoparticles and controlled with low frequency alternating magnetic field. Theranostics 7 (13), 3326–3337.

Caras, S.D., Petelenz, D., Janata, J., 1985. Ph-based nzyme potentiometric sensors .2. Glucose-sensitive field-effect transistor. Anal. Chem. 57 (9), 1920–1923.

Chae, M.S., Yoo, Y.K., Kim, J., Kim, T.G., Hwang, K.S., 2018. Graphene-based enzyme-modified field-effect transistor biosensor for monitoring drug effects in Alzheimer's disease treatment. Sensor. Actuator. B Chem. 272, 448–458.

Chen, F., Xia, J., Ferry, D.K., Tao, N., 2009. Dielectric screening enhanced performance in graphene FET. Nano Lett. 9 (7), 2571–2574.

Chen, X.Y., Hao, S.B., Zong, B.Y., Liu, C.B., Mao, S., 2019a. Ultraselective antibiotic sensing with complementary strand DNA assisted aptamer/MoS2 field-effect transistors. Biosens. Bioelectron. 145, 111711–111721.

Chen, X.Y., Liu, Y., Fang, X., Li, Z., Pu, H.H., Chang, J.B., Chen, J.H., Mao, S., 2019b. Ultratrace antibiotic sensing using aptamer/graphene-based field-effect transistors. Biosens. Bioelectron. 126, 664–671.

Cheung, K.M., Yang, K.A., Nakatsuka, N., Zhao, C., Ye, M., Jung, M.E., Yang, H., Weiss, P. S., Stojanovic, M.N., Andrews, A.M., 2019. Phenylalanine monitoring via aptamer-field-effect transistor sensors. ACS Sens. 4 (12), 3308–3317.

Choi, Y., Yau, S.T., 2009. Field-effect enzymatic amplifying detector with picomolar detection limit. Anal. Chem. 81 (16), 7123–7126.

Elnathan, R., Kwiat, M., Pevzner, A., Engel, Y., Burstein, L., Khatchtourints, A., Lichtenstein, A., Kantaev, R., Patolsky, F., 2012. Biorecognition layer engineering: overcoming screening limitations of nanowire-based FET devices. Nano Lett. 12 (10), 5245–5254.

Fan, Z., Ho, J.C., Jacobson, Z.A., Yerushalmi, R., Alley, R.L., Razavi, H., Javey, A., 2008. Wafer-scale assembly of highly ordered semiconductor nanowire arrays by contact printing. Nano Lett. 8 (1), 20–25.

Gao, A., Lu, N., Wang, Y., Dai, P., Li, T., Gao, X., Wang, Y., Fan, C., 2012. Enhanced sensing of nucleic acids with silicon nanowire field effect transistor biosensors. Nano Lett. 12 (10), 5262–5268.
Gao, X.P., Zheng, G., Lieber, C.M., 2010. Subthreshold regime has the optimal sensitivity for nanowire FET biosensors. Nano Lett. 10 (2), 547–552.
Garrido, J.A., Härtl, A., Dankerl, M., Reitinger, A., Eickhoff, M., Helwig, A., Müller, G., Stutzmann, M., 2008. The surface conductivity at the Diamond/aqueous electrolyte interface. J. Am. Chem. Soc. 130, 4177–4181.
Hafez, M.E., Ma, H., Ma, W., Long, Y.T., 2019. Unveiling the intrinsic catalytic activities of single-gold-nanoparticle-based enzyme mimetics. Angew Chem. Int. Ed. Engl. 58 (19), 6327–6332.
Hammock, M.L., Knopfmacher, O., Ng, T.N., Tok, J.B.H., Bao, Z.A., 2014. Electronic readout enzyme-linked immunosorbent assay with organic field-effect transistors as a preeclampsia prognostic. Adv. Mater. 26 (35), 6138–6148.
Hartl, A., Baur, B., Stutzmann, M., Garrido, J.A., 2008. Enzyme-modified field effect transistors based on surface-conductive single-crystalline diamond. Langmuir 24 (17), 9898–9906.
He, W., Liu, R., Zhou, P., Liu, Q., Cui, T., 2020. Flexible micro-sensors with self-assembled graphene on a polyolefin substrate for dopamine detection. Biosens. Bioelectron. 167, 112473–112481.
Kamahori, M., Ishige, Y., Shimoda, M., 2007. A novel enzyme immunoassay based on potentiometric measurement of molecular adsorption events by an extended-gate field-effect transistor sensor. Biosens. Bioelectron. 22 (12), 3080–3085.
Kergoat, L., Piro, B., Berggren, M., Horowitz, G., Pham, M.C., 2012. Advances in organic transistor-based biosensors: from organic electrochemical transistors to electrolyte-gated organic field-effect transistors. Anal. Bioanal. Chem. 402 (5), 1813–1826.
Khoshfetrat, S.M., Mehrgardi, M.A., 2017. Amplified detection of leukemia cancer cells using an aptamer-conjugated gold-coated magnetic nanoparticles on a nitrogen-doped graphene modified electrode. Bioelectrochemistry 114, 24–32.
Kwon, O.S., Park, S.J., Hong, J.Y., Han, A.R., Lee, J.S., Lee, J.S., Oh, J.H., Jang, J., 2012. Flexible FET-type VEGF aptasensor based on nitrogen-doped graphene converted from conducting polymer. ACS Nano 6 (2), 1486–1493.
Lei, Y., Butler, D., Lucking, M.C., Zhang, F., Xia, T., Fujisawa, K., Granzier-Nakajima, T., Cruz-Silva, R., Endo, M., Terrones, H., Terrones, M., Ebrahimi, A., 2020. Single-atom doping of MoS2 with manganese enables ultrasensitive detection of dopamine: experimental and computational approach. Sci Adv 6 (32), 4250–4255.
Li, J., Yang, C., Wang, W.L., Yan, X.P., 2018. Functionalized gold and persistent luminescence nanoparticle-based ratiometric absorption and TR-FRET nanoplatform for high-throughput sequential detection of l-cysteine and insulin. Nanoscale 10 (31), 14931–14937.
Li, J., Zhang, Y., To, S., You, L., Sun, Y., 2011. Effect of nanowire number, diameter, and doping density on nano-FET biosensor sensitivity. ACS Nano 5 (8), 6661–6668.
Li, N., Nan, C., Mei, X., Sun, Y., Feng, H., Li, Y., 2020. Electrochemical sensor based on dual-template molecularly imprinted polymer and nanoporous gold leaf modified electrode for simultaneous determination of dopamine and uric acid. Mikrochim. Acta 187 (9), 496–502.
Magliulo, M., Manoli, K., Macchia, E., Palazzo, G., Torsi, L., 2015. Tailoring functional interlayers in organic field-effect transistor biosensors. Adv. Mater. 27 (46), 7528–7551.
Mao, S., Chang, J., Pu, H., Lu, G., He, Q., Zhang, H., Chen, J., 2017. Two-dimensional nanomaterial-based field-effect transistors for chemical and biological sensing. Chem. Soc. Rev. 46 (22), 6872–6904.
Melzer, K., Bhatt, V.D., Jaworska, E., Mittermeier, R., Maksymiuk, K., Michalska, A., Lugli, P., 2016. Enzyme assays using sensor arrays based on ion-selective carbon nanotube field-effect transistors. Biosens. Bioelectron. 84, 7–14.
Nakatsuka, N., Yang, K.A., Abendroth, J.M., Cheung, K.M., Xu, X., Yang, H., Zhao, C., Zhu, B., Rim, Y.S., Yang, Y., Weiss, P.S., Stojanovic, M.N., Andrews, A.M., 2018. Aptamer-field-effect transistors overcome Debye length limitations for small-molecule sensing. Science 362 (6412), 319–324.
Ogata, K., Koike, K., Tanite, T., Komuro, T., Sasa, S., Inoue, M., Yano, M., 2004. High resistive layers toward ZnO-based enzyme modified field effect transistor. Sensor. Actuator. B Chem. 100 (1–2), 209–211.
Ordinario, D.D., Burke, A.M., Phan, L., Jocson, J.M., Wang, H.F., Dickson, M.N., Gorodetsky, A.A., 2014. Sequence specific detection of restriction enzymes at DNA-modified carbon nanotube field effect transistors. Anal. Chem. 86 (17), 8628–8633.
Park, S.J., Kwon, O.S., Lee, S.H., Song, H.S., Park, T.H., Jang, J., 2012. Ultrasensitive flexible graphene based field-effect transistor (FET)-type bioelectronic nose. Nano Lett. 12 (10), 5082–5090.
Rakovska, A., Javitt, D., Petkova-Kirova, P., Balla, A., Ang, R., Kalfin, R., 2019. Neurochemical evidence that cysteamine modulates amphetamine-induced dopaminergic neuronal activity in striatum by decreasing dopamine release: an in vivo microdialysis study in freely moving rats. Brain Res. Bull. 153, 39–46.
Singh, K., Lou, B.S., Her, J.L., Pang, S.T., Pan, T.M., 2019. Super Nernstian pH response and enzyme-free detection of glucose using solgel derived RuOx on PET flexible-based extended-gate field-effect transistor. Sensor. Actuator. B Chem. 298, 126837–126844.
Surya, S.G., Majhi, S.M., Agarwal, D.K., Lahcen, A.A., Yuvaraja, S., Chappanda, K.N., Salama, K.N., 2020. A label-free aptasensor FET based on Au nanoparticle decorated Co3O4 nanorods and a SWCNT layer for detection of cardiac troponin T protein. J. Mater. Chem. B 8 (1), 18–26.
Vasudevan, S., Kajtez, J., Bunea, A.I., Gonzalez-Ramos, A., Ramos-Moreno, T., Heiskanen, A., Kokaia, M., Larsen, N.B., Martinez-Serrano, A., Keller, S.S., Emneus, J., 2019. Leaky optoelectrical fiber for optogenetic stimulation and electrochemical detection of dopamine exocytosis from human dopaminergic neurons. Adv. Sci. 6 (24), 1902011–1902018.
Vijayalakshmi, A., Tarunashree, Y., Baruwati, B., Manorama, S.V., Narayana, B.L., Johnson, R.E.C., Rao, N.M., 2008. Enzyme field effect transistor (ENFET) for estimation of triglycerides using magnetic nanoparticles. Biosens. Bioelectron. 23 (11), 1708–1714.
Wu, W., Li, J., Pan, D., Li, J., Song, S., Rong, M., Li, Z., Gao, J., Lu, J., 2014. Gold nanoparticle-based enzyme-linked antibody-aptamer sandwich assay for detection of Salmonella Typhimurium. ACS Appl. Mater. Interfaces 6 (19), 16974–16981.
Yang, H.J., Song, H.J., Shin, H.J., Choi, H.C., 2005. A rapid synthesis of iron phosphate nanoparticles via surface-mediated spontaneous reaction for the growth of high-yield, single-walled carbon nanotubes. Langmuir 21 (20), 9098–9102.
Ye, Y., Ji, J., Pi, F., Yang, H., Liu, J., Zhang, Y., Xia, S., Wang, J., Xu, D., Sun, X., 2018. A novel electrochemical biosensor for antioxidant evaluation of phloretin based on cell-alginate/L-cysteine/gold nanoparticle-modified glassy carbon electrode. Biosens. Bioelectron. 119, 119–125.
Yoon, H., Ko, S., Jang, J., 2008. Field-effect-transistor sensor based on enzyme-functionalized polypyrrole nanotubes for glucose detection. J. Phys. Chem. B 112 (32), 9992–9997.
Zhang, L., Yuan, R., Chai, Y., Li, X., 2007. Investigation of the electrochemical and electrocatalytic behavior of positively charged gold nanoparticle and L-cysteine film on an Au electrode. Anal. Chim. Acta 596 (1), 99–105.